WARSAW UNIVERSITY OF TECHNOLOGY Index 351733
FACULTY OF CIVIL ENGINEERING
COMMITTEE FOR CIVIL AND WATER ENGINEERING
POLISH ACADEMY OF SCIENCES ISSN 1230-2945
DOI: 10.24425/ace.2026.158605
ARCHIVES OF CIVIL ENGINEERING
Vol. LXXII ISSUE 2 2026
pp. 215 –229

Research paper

Experimental study and numerical simulation of uniaxial compression on artificial rock samples with Z-shaped fractures

Liangxiao Xiong[1], Liyu Gong[2], Tao Zhou[3], Zhongyuan Xu[4], Deye Hu[5]

Abstract: To study the influence of the inclination and length of *Z*-shaped fissures on the mechanical properties and failure characteristics of the rock mass, this study conducts a series of uniaxial compression tests on rock-like materials with prefabricated *Z*-shaped fractures. In addition, two-dimensional Particle Flow Code software is used to perform uniaxial compression numerical simulations. The results show that: (1) Other parameters are the same, under different γ, the β had a significant impact on the change trend of the compressive strength and elastic modulus of the specimen, showing an "*M*-shaped". (2) Other parameters are the same,when $\beta \neq 0°$, the compressive strength and elastic modulus of the specimen are negatively correlated with γ, but $\beta = 0°$, then the two are positively correlated with γ. (3) Other parameters are the same, when $\gamma_a \neq 90°$, the trend of compressive strength and elastic modulus of the specimen showed an "*M*-shape" with the increase of β. But $\gamma_a = 90°$, the two are negatively correlated with β. (4) Other parameters are the same, under different β, the compressive strength and elastic modulus of the specimen are positively correlated with γ_a. (5) The main damage mode of *Z*-crack specimen is tensile shear damage.

Keywords: compressive strength, destruction mode, elastic modulus, numerical Simulation, Z-shaped fissure

[1]Associate Prof., PhD., Eng., School of Civil Engineering and Architecture, East China Jiaotong University, Nanchang 330013, China, e-mail: xionglx1982@126.com, ORCID: 0000-0002-6366-5187
[2]B.Eng., School of Civil Engineering and Architecture, East China Jiaotong University, Nanchang 330013, China, e-mail: 1211780250@qq.com, ORCID: 0009-0002-9769-5058
[3]Eng., College of Environment and Civil Engineering, Chengdu University of Technology, Chengdu, 610059, PR China, e-mail: 1312186954@qq.com, ORCID: 0000-0001-7153-9562
[4]PhD., Faculty of Geosciences and Environmental Engineering, Southwest Jiaotong University, Chengdu 611756, China, e-mail: zyxu@swjtu.edu.cn, ORCID: 0000-0003-4303-1870
[5]B.Eng., School of Civil Engineering and Architecture, East China Jiaotong University, Nanchang 330013, China, e-mail: 2573713909@qq.com, ORCID: 0000-0001-8132-0812

1. Introduction

Owing to the influence of geological structures and weathering, most rock masses in nature contain fissures of different shapes. The inclination of these cracks have a strong influence on the mechanical properties of the rock mass and also affect the stability in engineering practices. Thus, it is of great significance to test the mechanical properties and structural crack feature of rock masses.

The researchers have carried out a large number of experimental studies and numerical simulations on rock masses and rock-like materials containing prefabricated fractures. In terms of laboratory experiments, Wang et al. [1–3] prefabricated single-crack rock samples to study the mechanical properties, crack propagation, failure process, failure mechanism and energy evolution of single-crack rocks at different dip angles and thicknesses. Xiao et al. [4] studied the mechanical properties of prefabricated single-fault marble under different fault lengths and dip angles, and found that the failure mode was controlled by the fault dip angle and the fault degree. Zhou et al. [5] conducted experiments on coal and rock samples with different bedding dips to study their strength, failure modes and crack distribution. Chen et al. [6–8] studied the mechanical properties of different rocks by changing the length and angle of orthogonal cracks, and found that the crack length had little effect on the strength, and the tilt angle was the main reason for the peak strength. Wu et al. [9, 10] studied the mechanical properties and failure modes of cross-fractured rocks, and found that the cross-crack angle had little effect on the elastic modulus but had little effect on the peak strength, and the peak strength and elastic modulus of single-fractured rocks were greater than those of cross-fractures. Lai et al. [11] obtained the failure characteristics and cracking laws of single and composite rocks according to the failure process of composite rocks under high stress.

In terms of numerical simulations: Song et al. [12–14] used PFC to study the mechanical properties of rocks under different crack parameters, and the variation law of the stress-strain curve was basically consistent with the experimental results. Wang et al. [15] simulated uniaxial compressive failure of non-penetrating fractured rock samples based on PFC to explore the influence of rock bridge dip angle. He et al. [16] studied the mechanical properties of rock mass specimens with different pore sizes, and used PFC simulation to obtain uniaxial compressive strength and crack evolution law. Zhou et al. [17] used Rhino- Griddle modeling and FLAC3D to simulate the uniaxial compressive deformation and failure of fractured rock mass. Jia et al. [18] simulated uniaxial compression experiments of prefabricated three-fractured yellow sandstone to analyze the influence of its central crack dip angle. Wu et al. [19] built a rock material model based on uniaxial compression data to simulate the mechanical properties of single and double fractured rock samples at different dip angles. Tang et al. [20] carried out PFC numerical simulation on single-fracture rock samples, and found that under uniaxial compression conditions, the failure was tensile failure, and the main failure during unloading was shear failure.

As mentioned above, few scholars have studied the "Z-shaped" fracture structure that is common in actual slope engineering, so this paper conducts uniaxial compression test and uses PFC2D to construct a numerical model to explore the influence of crack angles on the mechanical properties of rock mass and structural fracture characteristics.

2. Indoor uniaxial compression test

2.1. Selection of sample materials

Cracks in natural rocks affect their physical and mechanical properties. In this study, cement, river sand, and water were mixed in specific proportions to make rock-like materials. The experimental cement was 32.5*R* ordinary Portland cement (the minimum value of 28 days compressive strength was 32.5 MPa, and the density was 3.0–3.15 g/cm^3). The specimen is a 100×100×100 mm cube. The prefabricated Z-shaped crack in the rock mass consists of the main fissure a and two parallel secondary fissures b, which are of different lengths but are both 1 mm wide. The uniaxial compressive strength and elastic modulus were obtained by uniaxial compression tests on the three complete specimens, and the density was obtained according to the mass and volume, and the macroscopic mechanical parameters of the three groups of complete specimens without prefabricated cracks were shown in Table 1.

Table 1. Mechanical parameters of intact specimens under uniaxial compression

Specimen number	**Compressive strength (MPa)**	**Elastic Modulus *E* (GPa)**	**Density ρ (g·cm–3)**
1	25.16	1.75	2.08
2	25.13	1.71	2.04
3	25.10	1.74	2.06
Average	25.13	1.73	2.06

2.2. Sample preparation

The thickness of cracks in all samples is about 1 mm. The position of the γ, γ_a and β of the prefabricated crack of the specimen is shown in Figure 1.

Sample preparation included the following steps. First, mixed material: The early-strength ordinary Portland cement (32.5*R*) with a strength grade of 32.5 MPa is mixed with fine river sand with a particle size of 0.25–0.45 mm and uniform particle size at a ratio of 1:2, and water is added to make the water-cement ratio reach 0.6. Second, pour into the mold: Pour the mixture into a mold with lubricated oil (for easy demoulding) and a size of 100×100×100 mm. Third, eliminate air bubbles: Place the mold on the vibrating table to remove air bubbles. Four, insert PVC sheets: Lubricate the transparent PVC sheets 12 mm long and 1 mm thick and insert the sample as planned. Fifth, demoulding treatment: After 12 h in the sample chamber, the PVC insert is taken out, and the mold is demolded after 24 h. Sixth, soak for later use: Put the sample in a storage box, soak it in water for 28 d, and then take it out for later use.

In this study, the prefabricated *Z*-type cracks of the specimen were divided into type A and type B. Both contain primary fissure a and two secondary parallel fissure b (b_1 and b_2). The inclination angle γ of the type A *Z*-shaped fracture is the clockwise angle between the vertical line of the main fissure and the secondary fissure, and the inclination angle β is the clockwise angle between the main fissure and the vertical line, as shown in Fig. 1a. The inclination angle γ_a of the type B *Z*-shaped fissure is the angle between the vertical line of the main fissure and the counterclockwise direction of the secondary fissure, as shown in Fig. 1b.

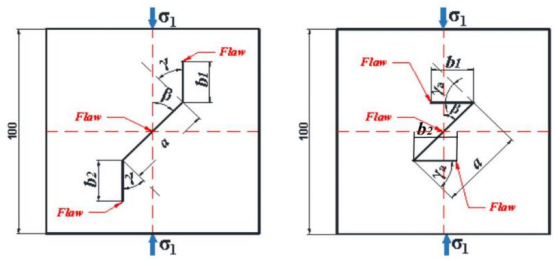

(a) (b)

Fig. 1. Schematic diagram of uniaxial compression on specimens with Z-shaped fracture (Unit: mm): a) Type A, b) Type B

Due to the numerous working conditions of this test specimen, the prefabricated fracture length $b_1 = b_2$ is selected for analysis in this paper, and all subsequent b refer to b_1 and b_2. The grouping working conditions for types A and B Z-shaped fracture specimens are shown in Table 2 and 3.

Table 2. Grouping conditions of type A Z-fractured samples

Study	γ (°)	β (°)	a **(mm)**	b **(**$b1$ **and** $b2$**) (mm)**
1	0	0, 30, 45, 60, 90	10, 20, 30, 40	10, 20, 30, 40
2	30	0, 30, 45, 60, 90	20	20
3	45	0, 30, 45, 60, 90	20	20
4	60	0, 30, 45, 60, 90	20	20
5	90	0, 30, 45, 60, 90	20	20

Table 3. Grouping conditions of type B Z-fractured samples

Study	γ (°)	β (°)	a **(mm)**	b **(**$b1$ **and** $b2$**) (mm)**
1	0	0, 30, 45, 60, 90	10, 20, 30, 40	10, 20, 30, 40
2	30	0, 30, 45, 60, 90	20	20
3	45	0, 30, 45, 60, 90	20	20
4	60	0, 30, 45, 60, 90	20	20
5	90	0, 30, 45, 60, 90	20	20

2.3. Test equipment and methods

In this study, the CSS-44300 electronic universal testing machine was used to compress the sample uniaxially at a loading rate of 1 mm/min by controlling the displacement. Set the parameters to collect data in 0.1 s increments and record images after the sample breakage.

3. Analysis of indoor test results

3.1. Stress-strain curve analysis

Figure 2 and 3 show uniaxial compression stress-strain curves of specimens with varied crack inclination angles when $a = b = 20$ mm.

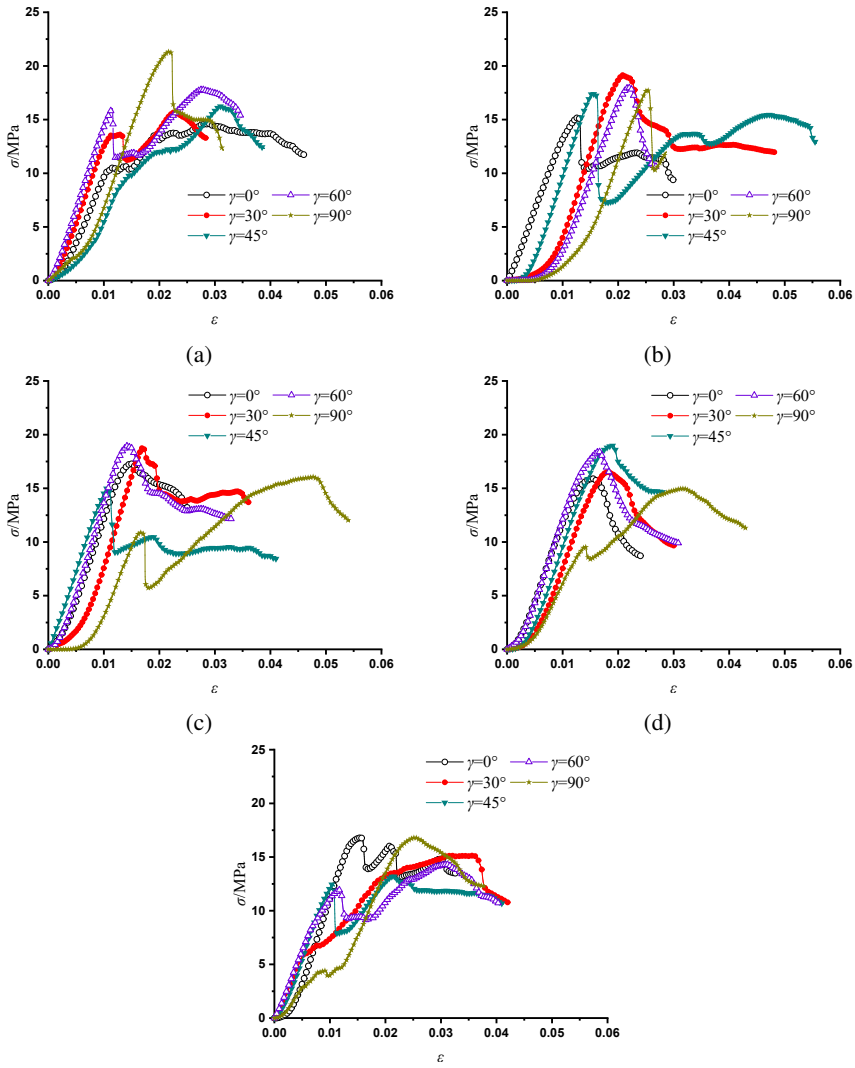

Fig. 2. Influence of β on the stress-strain curve of the specimen for each selected γ, $a = b = 20$ mm: (a) $\beta = 0°$, (b) $\beta = 30°$, (c) $\beta = 45°$, (d) $\beta = 60°$, (e) $\beta = 90°$

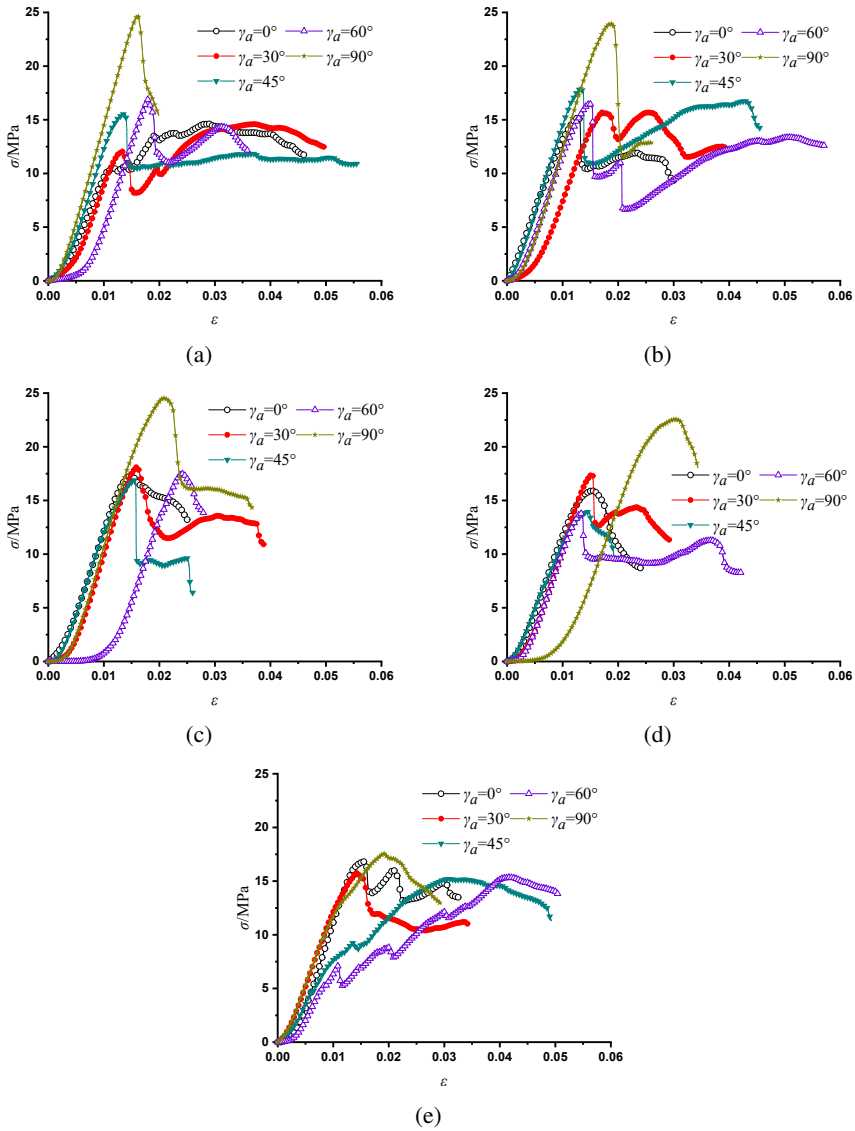

Fig. 3. Influence of β on the stress-strain curve of the specimen for each selected γ_a, $a = b = 20$ mm: : (a) $\beta = 0°$, (b) $\beta = 30°$, (c) $\beta = 45°$, (d) $\beta = 60°$, (e) $\beta = 90°$

In Fig. 2, γ and β affect the stress-strain curve of the specimen, but the regularity is not obvious. In Fig. 3, the peak stress is the largest and the curve changes most obviously if $\gamma = 90°$, the peak stress decreases with β increase. The peak stress is the lowest if $\beta = 90°$, because the load and crack direction change from the same direction to perpendicular, the resistance to failure in the same direction is the strongest, while the weakest in the vertical direction.

3.2. Influence of crack inclination on the compressive strength and elastic modulus of the rock mass

Figure 4 illustrates the influence of β on the compressive strength and elastic modulus of the sample when $a = b = 20$ mm and the γ values are varied.

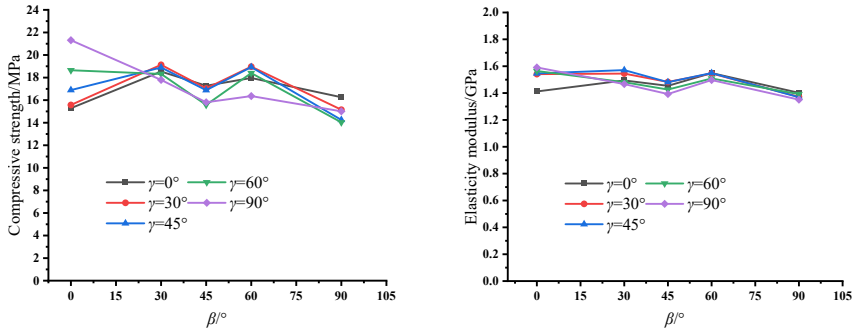

(a) (b)

Fig. 4. Influence of β on the uniaxial compressive strength (a) and elastic modulus (b) of the specimen for each selected γ ($a = b = 20$ mm)

All points in Fig. 4a are the peak points of the stress-strain curve (the uniaxial compressive strength of the specimen at different inclination angles) and Fig. 4b are the values of the slope of the linear elastic phase in the stress-strain curve (the elastic modulus of the crack specimen at different inclination angles). Two change trends are roughly same (because the compressive strength is positively correlated with the modulus of elasticity), and the line chart shows an "M-shaped" with β increase. Thus, the β had a significant impact on the change trend of the two in different γ if $a = b = 20$ mm, showing an "M-shaped".

Figure 5 shows the influence of γ on the compressive strength and elastic modulus of the cracked specimen when $a = b = 20$ mm did not change.

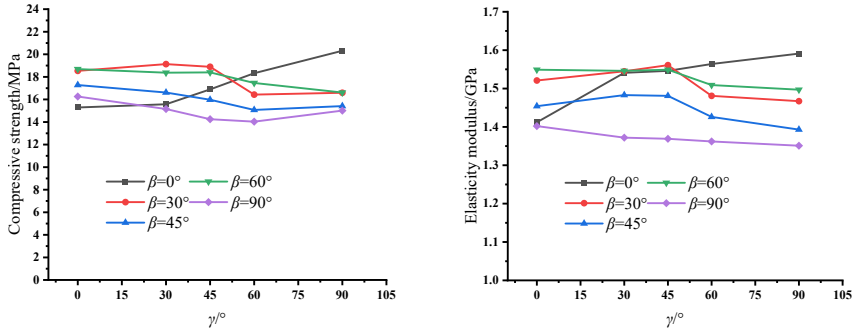

(a) (b)

Fig. 5. Influence of γ on the uniaxial compressive strength (a) and elastic modulus (b) of the specimen for each selected β ($a = b = 20$ mm)

In Fig. 5, the compressive strength and elastic modulus of the specimen decrease with γ increase (negative correlation) if $\beta \neq 0°$, because the crack is perpendicular to the load direction with γ increase, the ability of the specimen to resist failure decreases. The two increase with γ increase (positive correlation) if $\beta = 0°$, because the increase of γ makes the crack and the load direction tend to be consistent, the ability of the specimen to resist failure is enhanced.

Figure 6 shows the influence of β on the compressive strength and elastic modulus of the specimen when $a = b = 20$ mm remained unchanged and the γ_a was specified.

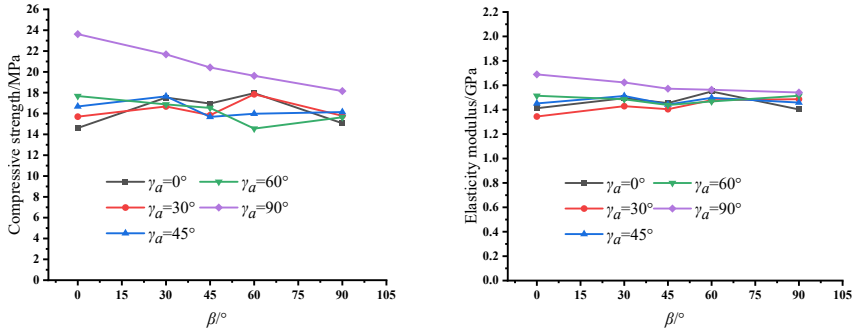

(a) (b)

Fig. 6. Influence of β on the uniaxial compressive strength (a) and elastic modulus (b) of the specimen for each selected $\gamma_a (a = b = 20$ mm)

In Fig. 6, the compressive strength and elastic modulus of the specimen show an "M-shaped" with the increase of β if $\gamma_a \neq 90°$. The two decrease with β increase (negative correlation) if $\gamma = 90°$, because the crack and the load direction gradually tend to be perpendicular in β increase, the compressive capacity of the specimen decreases.

Figure 7 shows the influence of γ_a on the peak strength and elastic modulus of the fractured rock mass when $a = b = 20$ mm remained unchanged and β was specified.

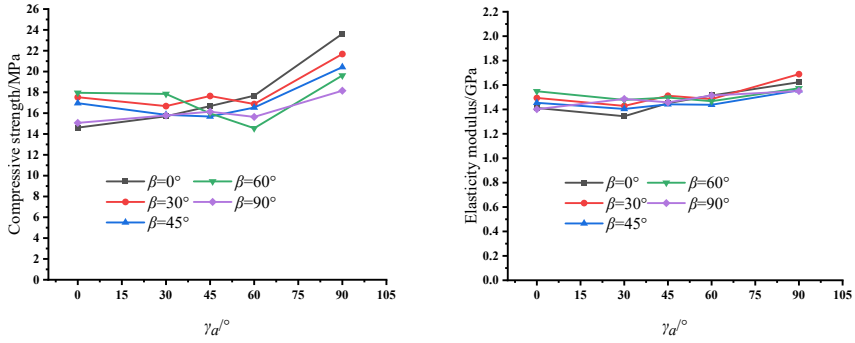

(a) (b)

Fig. 7. Influence of β on the uniaxial compressive strength (a) and elastic modulus (b) of the specimen, when γ and γ_a were the same ($a = b = 20$ mm)

In Fig. 7, γ_a increases from 0° to 90°, and the peak strength and elastic modulus of the specimen gradually increase (positive correlation). When $\gamma = 90°$, crack a coincides with b, and the peak strength and elastic modulus reach the maximum value in the range of $\gamma_a = 0° \sim 90°$.

4. Numerical simulation analysis

4.1. Parameter calibration

Referring to the macroscopic mechanical parameters of the uniaxial static load compression test, the microscopic parameters of the sample model were adjusted through multiple trial calculations, so that the microscopic parameters established by numerical simulation were basically consistent with the results of the uniaxial compression test, so as to complete the calibration of the microscopic parameters of the rock model. According to the test results of the crack sample of $\beta = \gamma = 0°$, the microscopic parameters of this numerical simulation were calibrated, and the parameter properties and contact types were determined after repeated debugging, as shown in Table 4.

Table 4. Mesoparameters used in numerical simulation of uniaxial compression

Parameter	**Numerical value**	**Parameter**	**Numerical value**
Minimum particle size (mm)	0.25	Bonding stiffness ratio (kn/ks)	1.5
density (g/cm^3)	1.96	Effective modulus (GPa)	1.4
Particle size ratio (Rmax/Rmin)	1.66	Coefficient of friction	0.4

These parameters were used to carry out multiple numerical simulation experiments on the four groups of samples under different working conditions. The numerical simulation results of the compressive strength and elastic modulus of the specimen are compared with the test results, as shown in Table 5 and 6.

Table 5. Numerical simulation results of compressive strength ($\beta = \gamma = 0°$, b = 10 mm)

nagłówek 1 **Study**	**Numerical simulation (MPa)**	**Indoor test (MPa)**	**Ratio of simulation results to test results**
a = 10 mm	14.21	19.39	0.732
a = 20 mm	13.53	17.53	0.771
a = 30 mm	12.70	16.69	0.761
a = 40 mm	12.17	15.8	0.770

Table 6. Numerical simulation results of elastic modulus
($\beta = \gamma = 0°$, $b = 10$ mm)

Study	Numerical simulation (GPa)	Indoor test (GPa)	Ratio of simulation results to test results
$a = 10$ mm	1.508	1.517	0.994
$a = 20$ mm	1.502	1.487	1.01
$a = 30$ mm	1.499	1.486	1.001
$a = 40$ mm	1.489	1.479	1.006

The results of compressive strength and elastic modulus obtained after numerous trial calculations are shown in Table 5 and 6, respectively. The compressive strength of the sample obtained through numerical simulation was about 76% of the indoor test compressive strength, and the elastic modulus result was close to that obtained in the indoor test.

PFC 2D was usd to be perform uniaxial compression numerical simulation on the specimens with different crack inclination angles. The particles at specified positions were deleted to simulate the prefabricated cracks in the sample. Figure 8 shows the indoor test and numerical simulation failure diagram of the sample when $\beta = \gamma = 0°$, $b = 10$ mm, and $a = 40$ mm.

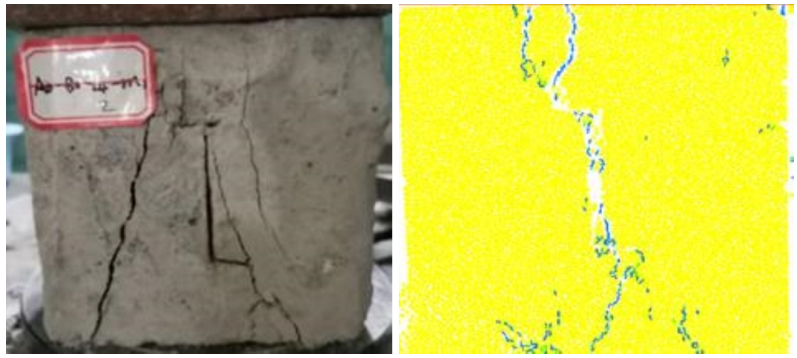

Fig. 8. Damage obtained during indoor testing and numerical simulation

In Fig. 8, the damage diagrams obtained by the indoor test and the numerical simulation of the sample were similar, and the extension direction and the location of the cracks are in good agreement.

Therefore, the parameters listed in Table 5 are reliable and can be used for accurate numerical simulation of uniaxial compression.

4.2. Analysis of numerical results

Figure 9 show the uniaxial compression numerical simulation results of the sample's compressive strength and elastic modulus when γ changed.

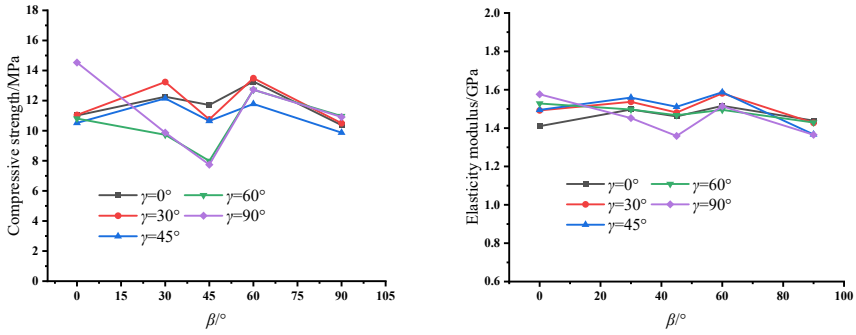

(a) (b)

Fig. 9. Numerical simulation results of various γ values against changes in β ($a = b = 20$ mm): (a) uniaxial compressive strength, (b) elastic modulus

In Fig. 9, when other parameters are the same, $\gamma = 0°$, 30° and 45°, the trend of compressive strength and elastic modulus of the specimen is "M-shaped" with the increase of β. At $\gamma = 60°$ and 90°, the compressive strength and elastic modulus of the specimen first decrease, then increase, and finally decrease. The results of numerical simulation show that the compressive strength of the specimen is consistent with the change trend of the elastic modulus.

5. Failure characteristic analysis

Figure 10 and 11 each respectively shows the final failure mode of the simulation model and the lab tests of samples with different β and γ values. Circled numbers 1-4 represent tensile cracks, tensile-shear mixed cracks, shear cracks and secondary inclined cracks, respectively.

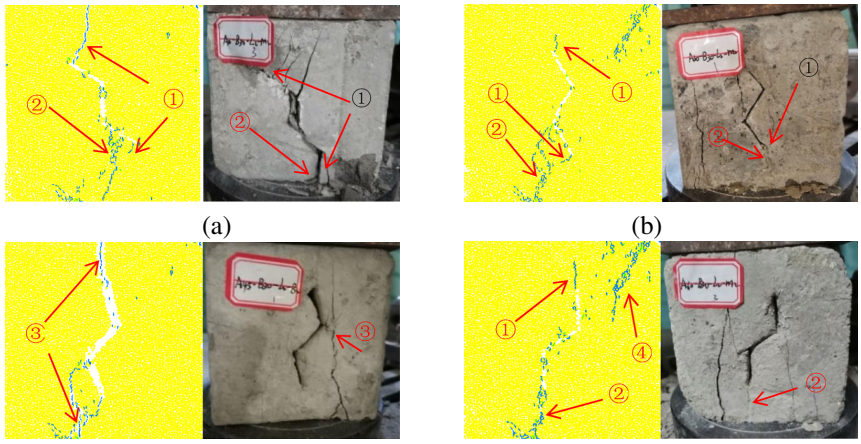

(a) (b)

(c) (d)

Figure continued on the next page

Figure continued from the previous page

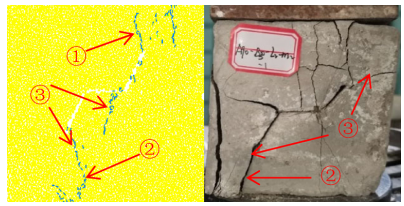

(e)

Fig. 10. Failure modes of samples with different β values ($a = b = 20$ mm, $\gamma = 30°$): (a) $\beta = 0°$, (b) $\beta = 30°$, (c) $\beta = 45°$, (d) $\beta = 60°$, (e) $\beta = 90°$

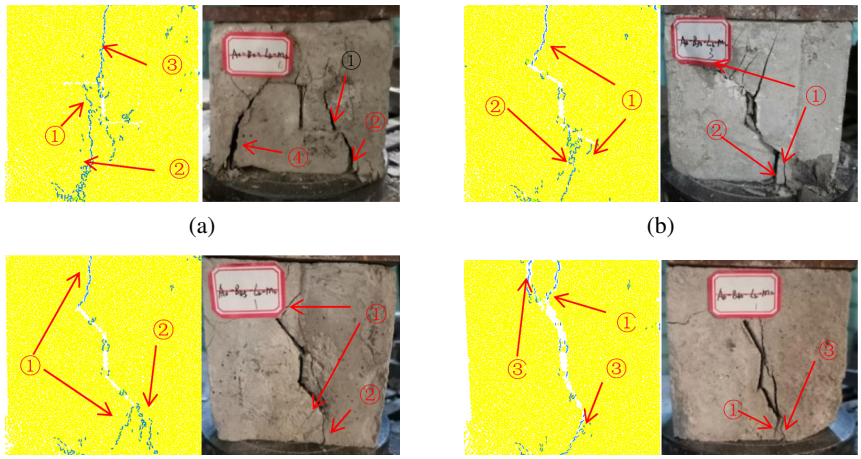

(a) (b)

(c) (d)

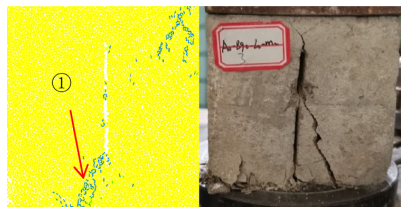

(e)

Fig. 11. Failure modes of samples with different of γ values ($a = b = 20$ mm, $\beta = 0°$): (a) $\beta = 0°$, (b) $\beta = 30°$, (c) $\beta = 45°$, (d) $\beta = 60°$, (e) $\beta = 90°$

During the compression failure of specimens with Z-shaped cracks, most cracks initiated at the crack tips and propagated to the specimen boundaries. The cracks were categorized into four types based on stress: tensile cracks at the crack tips due to stress concentration, tensile-shear mixed cracks at the ends from combined tensile and shear stresses, shear cracks at the ends from shear stress, and secondary inclined cracks.

The crack types in the specimens shown in Fig. 10a and Fig. 11a–c are mainly tensile cracks and tensile-shear mixed cracks. But in Fig. 10b–e and Fig. 11d exhibit a large inclination angle relative to the horizontal direction, which indicate shear cracks. Moreover, the prefabricated crack direction of the sample shown in Fig. 11e coincides with the load direction, indicating tensile cracks.

According to the different types of cracks through the fracture surface in the sample, the failure modes of the samples with different Z-shaped cracks can be divided into the following three types.

5.1. Tensile failure

This failure mode is caused by the tensile crack propagation connecting the upper and lower surfaces of the sample to form a tensile through fracture surface that causes the sample to be damaged. The sample with $\gamma = 90°$ in Fig. 11 exhibits this failure mode.

5.2. Tensile-shear mixed failure

This failure mode is caused by the tensile-shear mixed crack propagation to form a through fracture surface that causes the specimen to fail. According to the different crack penetration failure positions in the sample, this failure occurs under the following four conditions.

Tensile cracks are generated from or near the left tip of crack b_1 and propagate upward to the upper boundary or downward to the lower boundary of the specimen. Three different mechanisms are involved in the follow case. The first begins at the right tip of b_2, where a tensile-shear crack propagates downward and penetrates the lower boundary. This type is exhibited in the sample with $\gamma = 45°$. The second begins at the right tip of b_2, where a shear crack propagates through the lower boundary. This type is exhibited in the sample with $\beta = 0°$ and $\gamma = 60°$. The third begins at lower tip of the main fissure, where a tensile-shear crack is generated and spreads downward to penetrate the lower boundary. This type is exhibited in the sample with $\beta = 30°$. Finally, tensile cracks are generated from the right tip of b_1 and extend upward to the upper boundary, and tensile-shear cracks generated from the middle part of b_1 extend downward to the lower boundary. This was observed in the samples with $\gamma = 0°$.

5.3. Shear failure

From the left tip of b_1, the specimen produced a shear crack that expanded upward to the upper boundary. From the right tip of b_2, a shear crack was generated that expanded downward, penetrated the lower boundary, then formed a through fracture surface with the prefabricated crack to destroy the specimen. This failure mode is shear failure and occurred in specimens with $\beta = 45°$.

In summary, most of the failure modes of the specimens with Z-shaped cracks examined in the present study were different forms of tensile-shear failure.

6. Conclusions

Through uniaxial compression test and numerical simulation of rock specimens containing Z-type prefabricated fractures, the following conclusions are obtained:

1. When other parameters are the same, the β had a significant impact on the compressive strength and elastic modulus of the specimen in different γ, and the curve is "M-shaped".
2. When other parameters are the same, the compressive strength and elastic modulus of the specimen are negatively correlated with γ in $\beta \neq 0°$, while positively correlated with γ in $\beta = 0°$.
3. When other parameters are the same, the trend of compressive strength and elastic modulus of the specimen in $\gamma_a \neq 90°$ showed an "M-shape" with β increase, while the two are negatively correlated with β if $\gamma = 90°$.
4. When other parameters are the same, the compressive strength and elastic modulus of the specimen in different β are positively correlated with γ_a.
5. The main damage mode of Z-crack specimen is tensile shear damage.

Acknowledgments

This work was supported by the Open Research Fund of State Key Laboratory of Geohazard Prevention and Geoenvironment Protection (Grant no. SKLGP2021K020) and the Open Research Fund of Engineering Research Center of Underground Mine Construction, Ministry of Education (Grant No. JYBGCZX2020101).

References

[1] C.P. Wang, et al., "Mechanical Properties and Failure Characteristics of Granite Intersected with Single Fractures Under Uniaxial Compression", *Journal of Southwest Jiaotong University*, vol. 59, no. 02, pp. 369–376+446, 2024, doi: 10.3969/j.issn.0258-2724.20230169.

[2] X.W. Zhang, et al., "On Mechanical Properties and Energy Evolution Anisotropy of Layered Rocks", *Journal of Hunan University of Science and Technology (Natural Science Edition)*, vol. 38, no. 02, pp. 1–9, 2023, doi: 10.13582/j.cnki.1672-9102.2023.02.001.

[3] Y. Liu, et al., "Influence of Crack Thickness and Angles on Mechanical Properties of Rock-Like Specimens", *Journal of Shaoxing University*, vol. 42, no. 10, pp. 26–34, 2022, doi: 10.16169/j.issn.1008-293x.k.2022.10.004.

[4] T.L. Xiao, et al., "Crack initiation characteristics and propagation law of marble-like rock under uniaxial compression", *Water Resources and Hydropower Engineering*, vol. 53, no. 08, pp. 161–171, 2022, doi: 10.13928/j.cnki.wrahe.2022.08.016.

[5] Y. Zhou, et al., "A meso-level study on mechanical properties of bedding coal under uniaxial compression", *Journal of Central South University (Science and Technology)*, vol. 53, no. 10, pp. 4036–4047, 2022, doi: 10.11817/j.issn.1672-7207.2022.10.023.

[6] Y.S. Chen, et al., "Experimental study on failure modes and mechanical properties of crisscross fractured rock samples under uniaxial compression conditions", *Journal of Experimental Mechanics*, vol. 35, no. 03, pp. 511–520, 2020, doi: 10.7520/1001-4888-18-194.

[7] Z.X. Lu and W. Wan, "Experimental Research on Rock-Like Materials with Orthogonally Crossed Cracks Under Uniaxial Compression", *Mineral Engineering Research*, vol. 38, no. 02, pp. 23–28, 2023, doi: 10.13582/j.cnki.1674-5876.2023.02.004.

[8] X. Wu, et al., "Experimental investigation on the strength characteristics and fracture mechanism of rock with orthogonally crossed cracks", *Journal of China Coal Society*, vol. 45, no. 07, pp. 2681–2690, 2020, doi: 10.13225/j.cnki.jccs.2020.0156.

[9] X. Wu, et al., "Deformation and energy evolution analysis of granite with cross-cracks under uniaxial compression", *Journal of Beijing Jiaotong University*, vol. 45, no. 03, pp. 77–83, 2021, doi: 10.11860/j.issn.1673-0291.20200139.

[10] S.C. Shen, et al., "Cross Fractured Sandstone Samples Uniaxial Mechanical Properties and Fracture Extended Failure", S*cience Technology and Engineering*, vol. 24, no. 09, pp. 3766–3772, 2024, doi: 10.12404/j.issn.1671-1815.2303930.

[11] Y.Z. Lai, et al., "Experimental Study on Uniaxial Compression Mechanics and Failure Characteristics of Composite Rocks", *Gold Science and Technology*, vol. 30, no. 05, pp. 778–786, 2022, doi: 10.11872/j.issn.1005-2518.2022.05.053.

[12] L. Song, et al., "Particle flow simulation of the effect of characteristics of filled joints on rock mechanical behavior under static compression", *Acta Scientiarum Naturalium Universitatis Sunyatseni*, vol. 62, no. 05, pp. 145–156, 2023, doi: 10.13471/j.cnki.acta.snus.2023d007.

[13] Y.L. Gao, et al., "Numerical Simulation Study on Uniaxial Compression of Fractured Rocks", *Journal of Henan University of Urban Construction*, vol. 32, no. 05, pp. 8–13, 2023, doi: 10.14140/j.cnki.hncjxb.2023.05.002.

[14] S.X. Liu, et al., "Experimental and Numerical Simulation Study on Mechanical Properties of Sandstone with Prefabricated Intermittent Fissures", *Water Resources and Power*, vol. 41, no. 04, pp. 181–185, 2023, doi: 10.20040/j.cnki.1000-7709.2023.20220195.

[15] X.J. Wang and S.B. Pi, "Study on the mechanical properties and energy evolution mechanism of non-penetrating fractured rock mass under uniaxial compression", *Gansu Water Resources and Hydropower Technology*, vol. 57, no. 05, pp. 26–30, 2021, doi: 10.19645/j.issn2095-0144.2021.05.008.

[16] B.Y. He, et al., "Uniaxial Compression Experiment and Numerical Simulation of Rock Bodies with Double Circular Holes of Equal Diameter", *Bulletin of the Chinese Ceramic Society*, vol. 39, no. 10, pp. 3213–3220, 2020, doi: 10.16552/j.cnki.issn1001-1625.2020.10.020.

[17] L. Zhou, et al., "Study on the influence of fracture geometry on rock mechanical properties under uniaxial compression", *Mining Technology*, vol. 24, no. 01, pp. 30–35, 2024, doi: 10.13828/j.cnki.ckjs.2024.01.015.

[18] D.W. Jia, et al., "Experimental Study on Mechanical Properties and Crack Propagation of Three-fissure Yellow Sandstone under Uniaxial Compression", *Journal of Hebei Institute of Architectural Engineering*, vol. 37, no. 04, pp. 56–61, 2019, doi: 10.3969/j.issn.1008-4185.2019.04.012.

[19] Y. Wu, et al., "Numerical and Experimental Study on Rock Containing Pre- existing Cracks Under Uniaxial Compression", *Journal of China Three Gorges University (Natural Sciences)*, vol. 43, no. 02, pp. 35–41, 2021, doi: 10.13393/j.cnki.issn.1672-948x.2021.02.007.

[20] Y. Tang, et al., "Conventional triaxial loading and unloading test and PFC numerical simulation of rock with single fracture", *Archives of Civil Engineering*, vol. 70, no. 2, pp. 233–254, 2024, doi: 10.24425/ace.2024.149861.

Received: 2023-08-09, Revised: 2024-09-26